Varying Assay Geometry to Emulate Connective Tissue Planes in an *In Vitro* Model of Acupuncture Needling

MARGARET JULIAS,[1] HELEN M. BUETTNER,[1,2] AND DAVID I. SHREIBER[2]*
[1]Department of Chemical and Biochemical Engineering, Rutgers, The State University of New Jersey, Piscataway, New Jersey
[2]Department of Biomedical Engineering, Rutgers, The State University of New Jersey, Piscataway, New Jersey

ABSTRACT

During traditional acupuncture, fine needles are inserted subcutaneously and rotated, which causes loose fascial tissue to wind around the needle. This coupling is stronger at acupuncture points, which tend to fall above intermuscular fascial planes, than control points, which lay above skeletal muscle. These different anatomical constraints may affect the mechanical coupling. Fascia at acupuncture points is bounded on two sides by skeletal muscle, but at control points is essentially unbounded. These differences were approximated in simple *in vitro* models. To emulate the narrower boundary within the intermuscular plane, type I collagen was cast in circular gels of different radii. To model the channel-like nature of these planes, collagen was cast in elliptical gels with major and minor axes matching the large and small circular gels, respectively, and in planar gels constrained on two sides. Acupuncture needles were inserted into the gels and rotated via a computer-controlled motor while capturing the evolution of fiber alignment under cross-polarization. Small circular gels aligned faster, but failed earlier than large circular gels. Rotation in elliptical and planar gels generated more alignment-per-revolution than circular gels. Planar gels were particularly resistant to failure. Fiber alignment in circular gels was isotropic, but was stronger in the direction of the minor axis in elliptical and planar gels. In fibroblast-populated gels, cells followed the alignment of the collagen fibers, and also became denser in regions of stronger alignment. These results suggest that the anatomy at acupuncture points provides unique boundaries that accentuate the mechanical response to needle manipulation. Anat Rec, 294:243–252, 2011. © 2010 Wiley-Liss, Inc.

Key words: acupuncture; connective tissue; fascia; tissue mechanics

INTRODUCTION

Although acupuncture has been clinically proven in treating conditions such as pain, nausea, and hypertension (NIH Consensus Statement, 1997) and has been increasingly used by patients seeking alternative medical therapies (Eisenberg et al., 1998), the mechanisms that underlie the therapeutic benefits remain unknown. During treatment, fine needles are inserted and rotated at specific locations on the body known as acupuncture points based on empirical maps passed down for centuries. Manipulating these acupuncture points is believed to regulate the flow of energy or "qi" through acupuncture meridians to produce local effects and specific, far-

Grant sponsor: National Institutes of Health; Grant number: R03 EB006045-01A1; Grant sponsor: New Jersey Commission on Spinal Cord Research; Grant number: 05-2912-SCR-E-0.

*Correspondence to: David I. Shreiber, Department of Biomedical Engineering, Rutgers, The State University of New Jersey, Piscataway, NJ 08854. Fax: 732-445-3753. E-mail: shreiber@rci.rutgers.edu

Received 11 December 2009; Accepted 20 September 2010
DOI 10.1002/ar.21308
Published online 3 December 2010 in Wiley Online Library (wileyonlinelibrary.com).

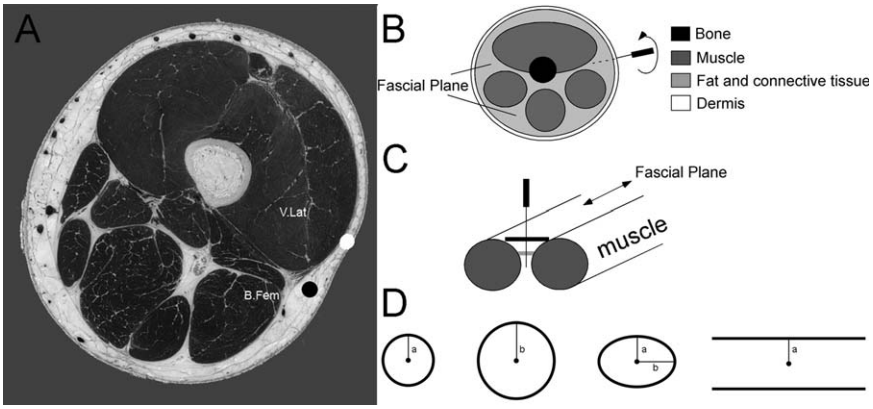

Fig. 1. (**A**) Anatomical section of a thigh (adapted from Langevin and Yandow, 2002). The white dot located above the vastus lateralis (V. Lat) represents a control point. The black dot located between the V. Lat and the biceps femoris (B. Fem) above an intermuscular cleavage plane, or fascial plane, indicates an acupuncture point. (**B**) Simplified schematic of a cross-section of the thigh indicating different tissue types and the location of fascial planes. (**C**) Along the axis of the muscles, the fascial plane presents a geometry that is generally bounded on two sides and narrows with increasing depth. (**D**) Simple assay geometries emulating the basic features of the fascial planes were generated out of PPE to create geometric constraints: two circles of different diameter to examine the effects of a narrowing boundary condition, and elliptical and planar geometries to simulate the anisotropic boundary conditions where the distance to the PPE constraints is greater in one direction. The line in the center of each configuration represents the smaller (a) or larger (b) radius.

reaching results. Despite the evidence for clinical and functional efficacy, there has been little correlation of acupuncture points and meridians to neuroanatomical structures or, until recently, physiological features.

Clinically, practitioners locate acupuncture points by identifying a nearby anatomical landmark, such as a bony prominence, muscle, or tendon, and then using light palpation to precisely determine the final position (Langevin and Yandow, 2002). Recently, Langevin and Yandow identified a high correlation between intermuscular and intramuscular connective tissue cleavage planes and acupuncture points (~80%) and meridians (~50%) by mapping acupuncture points on a cadaver to serial gross sections from the Visible Human Project (Fig. 1; Langevin and Yandow, 2002). At these points, there is an abundance of loose, interstitial, connective tissue and no underlying skeletal muscle. After locating the points, practitioners insert and manipulate the needles until they feel "needle grasp"—described as a "fish biting on a line"—at which time the patient senses "de qi" (Langevin et al., 2001b). Using an instrumented needling apparatus, Langevin showed that this grasping force at acupuncture points was significantly greater than at control points, which did not lie above connective tissue planes. Separate work with full-thickness rat abdominal wall explants, where acupuncture needles were inserted through epidermis, dermis, subcutaneous connective tissue and fat, and subcutaneous muscle and then rotated, demonstrated that only the loose, subcutaneous connective tissue wound around the needle to evoke a grasping force (Langevin et al., 2002). Working with explants of subcutaneous connective tissue alone, Langevin also showed that fibroblasts residing several millimeters away respond to the mechanical perturbation produced by acupuncture needle rotation with distinct morphological and cytoskeletal changes (Langevin et al., 2005).

Taken together, these results suggest that mechanical forces may contribute to the cellular and tissue changes leading to therapeutic benefits following acupuncture needling, and that the anatomical organization of soft tissues strongly influences the biomechanical response. However, untangling the contributions of these and other factors to the biophysical responses of tissues and cells in clinical settings or in explant studies, which present complex tissue environments, is difficult. We have developed a three-dimensional (3D) *in vitro* approach to examine the biophysical and, ultimately, the cellular responses to acupuncture needling in a controlled setting. Using type I collagen gels as tissue mimics, we demonstrated previously that the winding response of fibrillar collagen to needle rotation resembles that of loose connective tissue and varies with network density and stiffness and the depth of needle insertion (Julias et al., 2008).

In the current study, we used this *in vitro* approach to investigate the influence of fascial plane geometry on fiber winding. *In vivo*, the tissue in these planes is bounded on two sides by skeletal muscle, and generally becomes narrower with increasing depth to resemble a "V"-shaped channel, thereby, presenting distinct boundary conditions compared with locations above a muscle, which resembles an infinite plane (Fig. 1). We prepared circular gels of different radii to emulate the narrower boundary within the intermuscular plane, and elliptical gels and planar gels constrained on only two sides to model the anisotropic boundary conditions presented within these planes. We quantified the alignment response of fibers within these gels to controlled needling, and we examined cell alignment in fibroblast-populated gels.

MATERIALS AND METHODS

Collagen Gel Preparation

Collagen gel solutions were prepared from lyophilized collagen (Elastin Products, Owensville, MO) as previously described (Shreiber et al., 2001) to achieve a final

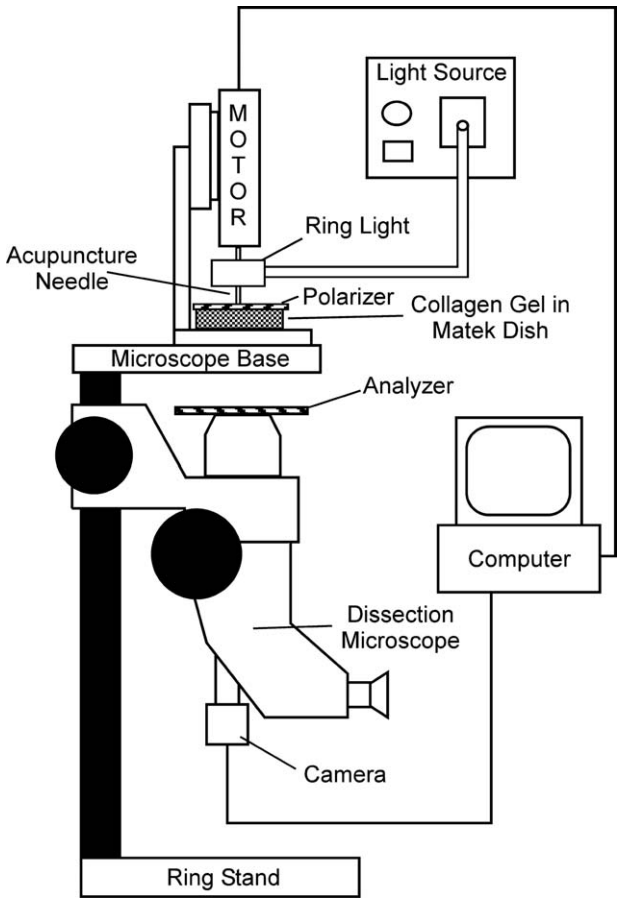

Fig. 2. Schematic of PLM system. A dissection stereomicroscope with a USB camera was mounted upside-down to a benchtop. A fiber-optic ring light was attached to the motor housing providing a light source to the sample without hindrance from the motor. The polarizer was placed on top of the sample dish, and the analyzer was placed on the microscope as shown with the axis of polarization orthogonal to the axis for the polarizer. A small hole in the polarizer allowed free insertion and rotation of the acupuncture needle in the sample. Originally published in Julias et al., 2008.

concentration of 2.5 mg/mL. The "V"-shaped geometry of a fascial plane presents two variations in geometry that affect the distance from the needle to the muscle wall, which in essence is the width of the loose connective tissue layer. These variations were emulated *in vitro*. First, the decrease in fascial plane width with increasing needle depth was modeled by casting collagen gels within circular hydrophilic porous polyethylene (PPE; Small Parts, Miramar, FL) annular inserts with different inner diameters, 28.6 mm and 19.1 mm. Second, the bounded plane, which presents a narrow channel of connective tissue, was modeled by preparing gels that extended farther in one axis than the other. These gels were either cast between two long (~35 mm—the width of the dish), thin strips of PPE placed 19.1 mm apart to capture the channel (termed "planar" gels), or within elliptical PPE inserts with major (28.6 mm) and minor (19.1 mm) diameters matching the large and small circular inserts, respectively (Fig. 1).

The collagen solution was poured into a 35-mm glass bottom MatTek dish with a 20-mm glass microwell (MatTek Corporation, Ashland, MA) containing the PPE inserts and incubated at 37°C for 4 hr to ensure complete fibril formation. The imaging approach (polarized light microscopy, described below) was strongly dependent on sample thickness within the imaged region. Accordingly, the gel centerline height was maintained at 4 mm for all conditions.

Cellular Gel Preparation

Cell-populated gels were prepared using rat dermal fibroblasts (RDFs) that were isolated and expanded from neonatal transgenic rats engineered to express green fluorescent protein (GFP; 488-nm excitation and 509-nm emission). RDFs were cultured in Dulbecco's Modified Eagle's Medium (Sigma Aldrich, St Louis, MO) supplemented with 10% fetal bovine serum (Atlanta Biologicals, Lawrenceville, GA), 2 mL of 200-mM L-glutamine (Sigma Aldrich, St Louis, MO), and 2 mL of 5,000 units/mL penicillin-5 mg/mL streptomycin (Sigma Aldrich, St Louis, MO). Trypsinized cells were rinsed in culture medium and resuspended in a 2-mg/mL collagen solution at a cell concentration of 100,000 cells/mL.

The *in vitro* setup was modified slightly to enhance cell viability within the tissue equivalent constructs by supporting the PPE annulus with short inserts to hold the gels above the bottom surface of the culture dish, which essentially suspended the gels within culture medium. The approach to create the suspended gels was not amenable to the planar gels, and cellular gels were only generated within large circular or elliptical inserts. First, a poly(dimethyl siloxane) (PDMS) template was created with a 60-mm outer diameter and an inner profile matching the shape of the PPE inserts. The PDMS template was placed in a 60-mm dish, and the PPE inserts were placed within the PDMS. The cell-containing collagen solution was poured into PPE ring and incubated at 37°C for 4 hr. Following self assembly, the PPE inserts with attached gels were removed from the PDMS and placed in a separate 60-mm dish on short PDMS support pegs, which introduced a small space between the bottom of the gel and the culture dish. The dish was filled with fresh culture medium, which allowed diffusive transport across both the top and bottom surfaces of the suspended gel and enhanced cell survival. After 2 days in culture, the PPE inserts and gels were transferred to a MatTek dish and covered with medium in preparation for controlled acupuncture needling.

In Vitro Acupuncture

A computer-controlled motor (MicroMo Electronics, Clearwater, FL) was used to needle the acellular and cellular collagen gels. For acellular gels, a 250-μm stainless steel acupuncture needle (Seirin, Tokyo, Japan) was attached to the motor and inserted perpendicular to the surface of the gel to a depth of 3 mm using a calibrated micromanipulator. The needle was rotated unidirectionally, which represents a form of needle manipulation often used clinically (Helms, 1995), for 10 revolutions at 0.3 rev/s, during which time the evolution of fiber alignment was continuously recorded with polarized light microscopy, as described below.

For cellular gels, the MatTek dish was first covered with a thin sheet of PDMS. The needle was inserted through the PDMS sheet and completely through the suspended gel. The cellular gels were needled for two revolutions at 0.3 rev/s. After needling, the needle was detached from the motor but remained in place because of the PDMS sheet, thereby, allowing the gel to be transferred to the stage of an inverted microscope for epifluorescent imaging of cell alignment without any unwinding or damage from needle removal. This approach to prevent needle movement was also used with a separate subset of acellular gels, which were exposed to 2.5 revolutions and then used to examine fiber alignment in different directions, as described below.

Polarized Light Imaging

Polarization light microscopy (PLM) was used to observe and image the evolution of fiber alignment continuously in real time, as previously described (Julias et al., 2008). A dissection stereomicroscope (Carl Zeiss Microimaging, Thornwood, NY) with a USB camera (Matrix Vision, GmbH, Oppenweiler, Germany) was physically inverted and clamped to a benchtop, which allowed the base of the microscope to be used as a platform to hold the motor stand and MatTek dish (Fig. 2). A fiber-optic ring light (Edmund Optics, Barrington, NJ) was attached to the motor housing. The gel was placed between two polarizers, which were positioned as "cross-polars" with their respective angles of polarization 90° apart. In this arrangement, as the light passes through the filter-sample-filter optic train, the darkest area of the resulting image occurs where collagen fibers are oriented parallel or perpendicular to the optical axis of either polarizing element; the brightest area occurs where collagen fibers are oriented 45° to the filters' optical axes. Initially, the axes of the polarizer and analyzer were aligned with the major and minor axes of the ellipse. Images were captured at six frames-per-second during needle rotation and were analyzed with MATLAB (The Mathworks, Natick, MA), as described below. To detect any anisotropy in the alignment pattern due to the asymmetric boundaries, in the subset of acellular gels where needling was stopped at 2.5 revolutions, samples were imaged under two additional polarization states. Specifically, the polarizer and analyzer were rotated 22.5° or 45° from the ellipse's major axis. The resulting birefringence is due to alignment ±45° from the axes of polarization (Fig. 3).

PLM Image Analysis

PLM-generated images were imported into MATLAB (The Mathworks, Natick, MA) to quantify the birefringence (Julias et al., 2008). The evolution of birefringence with needle rotation, reflecting the increase in the fiber alignment, was quantified by determining a continuous index of the alignment area using a thresholding algorithm, as previously described in detail (Julias et al., 2008). The alignment area was the area of pixels greater than or equal to the threshold intensity. At some point during the 10 revolutions, a tear develops within the gel, typically at the transition from circumferential alignment near the needle to radial alignment away from the needle. The hole in the gel is observed as an increasing black spot, which causes the alignment curves to decrease sharply and enabled determination of the number of revolutions before gel failure (Fig. 4).

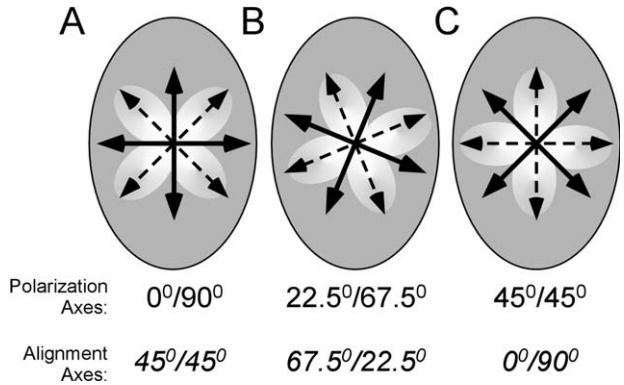

Fig. 3. The orientation of the axes of polarization (solid lines) with respect to the major and minor axes of the elliptical assay were rotated to assess fiber alignment in different directions (dashed lines/clover-leaf pattern). (**A**) When the polarization axes are coincident with the axes of the ellipse (0°/90°), fiber alignment is evaluated at 45°, which is symmetric with respect to the ellipse. The polarization axes are rotated to be 22.5°/67.5° (**B**) and 45°/45° (**C**) off of the axes of the ellipse to examine anisotropy in alignment.

Cell Alignment Quantification

Cell-populated gels were imaged before and after needle rotation. Needling was limited to two revolutions to prevent gel tearing. Gels were imaged with an Olympus IX81 inverted microscope (Olympus, Melville, NY) using 4× magnification and standard FITC optics to collect the GFP-generated fluorescent signal of cells within a ~2.0 mm^3 volume of gel. A motorized focus was used to capture 10 images at 50-μm intervals through the thickness of the sample in a ~2.25 × 1.75-mm^2 region centered around the needle. The images were coded with filenames that allowed them to be analyzed in a blinded fashion. Elliptical assays were oriented with the major axis horizontal to the captured image. Cell alignment was quantified from the images by tracing the major axis of a cell and determining the projection (cos θ) of the cell-axis vector to the radial position vector of its location with respect to the needle position (Fig. 5). These values were squared to produce an alignment index, $\Phi = \cos^2\theta$, for each cell, where $\Phi = 1$ indicated radial alignment and $\Phi = 0$ indicated circumferential alignment (Knapp et al., 1999). Only cells with distinct boundaries were traced, and the location of the cells within the image was marked and compared across images to ensure that a cell was not measured multiple times. Scatter plots of Φ with respect to centroid position were created to assess the spatial distribution of cell alignment. The total number of cells traced also served as a measure of cell density within the imaged volume.

Sample Sizes and Statistics

For acellular gel studies, 105 gels in total were subjected to *in vitro* acupuncture needling (N = 18–30 per assay configuration). Of those 105, needle rotation was stopped at 2.5 revolutions in 35 gels (N = 8–10 per assay configuration) to assess alignment nonuniformity by rotating the polarization axes. The remainder (N = 9–22 per configuration) were

needled until failure. For cellular gel studies, cell alignment was quantified within the ~2.0 mm^3 region around the needle in four circular gels and five elliptical gels for a total sample size of nine. The sample sizes for the different experiments are summarized in Table 1. Statistical comparisons were made among conditions using one-way ANOVA. When appropriate, posthoc pairwise comparisons were made with Hochberg's GT-2 method which is preferred when sample sizes are unequal (Sokal and Rohlf, 1981). Significance levels were set at $P < 0.05$.

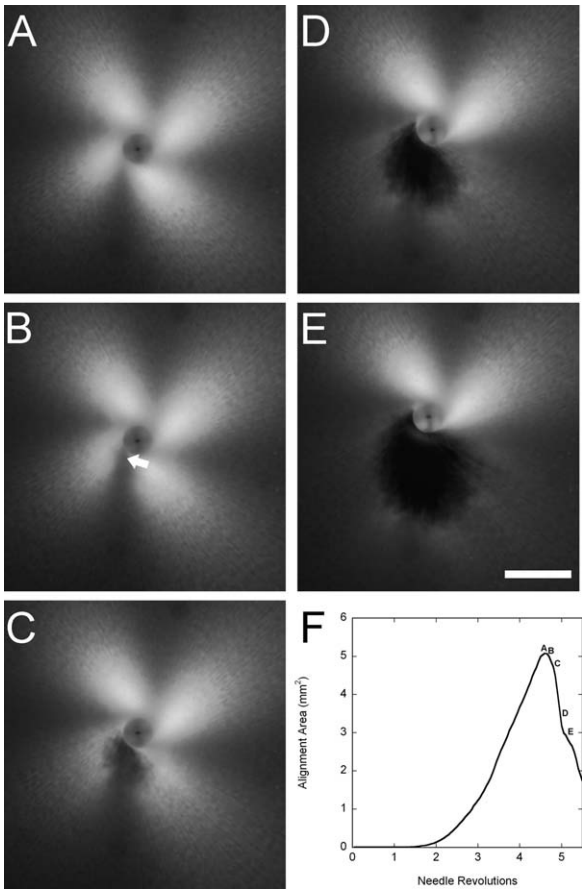

Fig. 4. Typical winding and failure of collagen gels during *in vitro* acupuncture. (**A**) PLM image of the gel immediately before the onset of tearing. The characteristic "four-leaf clover" pattern of birefringence increases in size up to the point of failure as the gel becomes increasingly aligned due to winding around the needle. (**B–E**) Development of gel failure at 0.5 sec (0.15 rev) intervals. At the onset of tearing (B), a weakening of the birefringence can be observed near the needle where the dense, circumferentially wound center transitions to radially aligned fibers (arrow). As failure ensues, a hole is observed in the gel (C–E). The increasing size of the tear results in a decreasing area of birefringence. (**F**) Images A–E marked on a plot of the area above a threshold intensity versus needle revolutions. The peak represents the image taken at maximum alignment immediately before the onset of failure. Bar: 1 mm. Adapted from previously published figure in Julias et al., 2008.

RESULTS

Effects of Assay Geometry on Fiber Winding

Rotating acupuncture needles within collagen gels cast in different geometries produced collagen fiber alignment that presented in a form of "four-leaf clover" using PLM (Fig. 6), which increased in area with increasing needle rotation. The alignment curves indicated that gels with anisotropic dimensions demonstrated more alignment than gels with uniform dimensions. Differences in alignment area at 2.4 revolutions, which represented the lowest number of revolutions before failure across all conditions, were statistically significant (ANOVA, $P < 0.001$; Fig. 7A). Posthoc pairwise comparisons confirmed that alignment at 2.4 revolutions was greater in gels with anisotropic dimensions than gels with uniform dimensions (Hochberg GT2 test, max $P = 0.005$), except when the planar gels were compared with the small circles ($P = 0.081$). Differences between the planar and elliptical gels were indistinguishable ($P = 0.992$). Smaller circular gels produced more alignment area than larger circular gels at 2.4 revolutions, though the results were not statistically significant following posthoc comparison ($P = 0.226$).

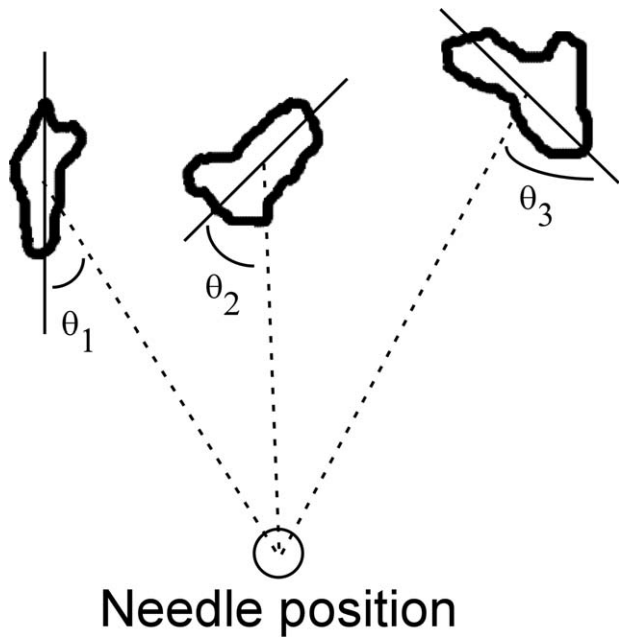

Fig. 5. Alignment was quantified for individual cells by projecting the long axis of the cell onto a radial vector connecting the centroid of the cell to the needle position to determine cos θ. These projections were squared to create an index, $\Phi = \cos^2 \theta$ ranging from 0 (circumferentially aligned) to 1 (radially aligned).

TABLE 1. Summary of Sample Sizes for the Various Experiments

Experiments	28.6-mm Circular gels	19.1-mm Circular gels	Elliptical gels	Planar gels
Fiber alignment until failure	N = 20	N = 21	N = 19	N = 9
Asymmetry of fiber alignment at 2.5 revolutions	N = 10	N = 9	N = 8	N = 9
Cell alignment	N = 4	–	N = 5	–

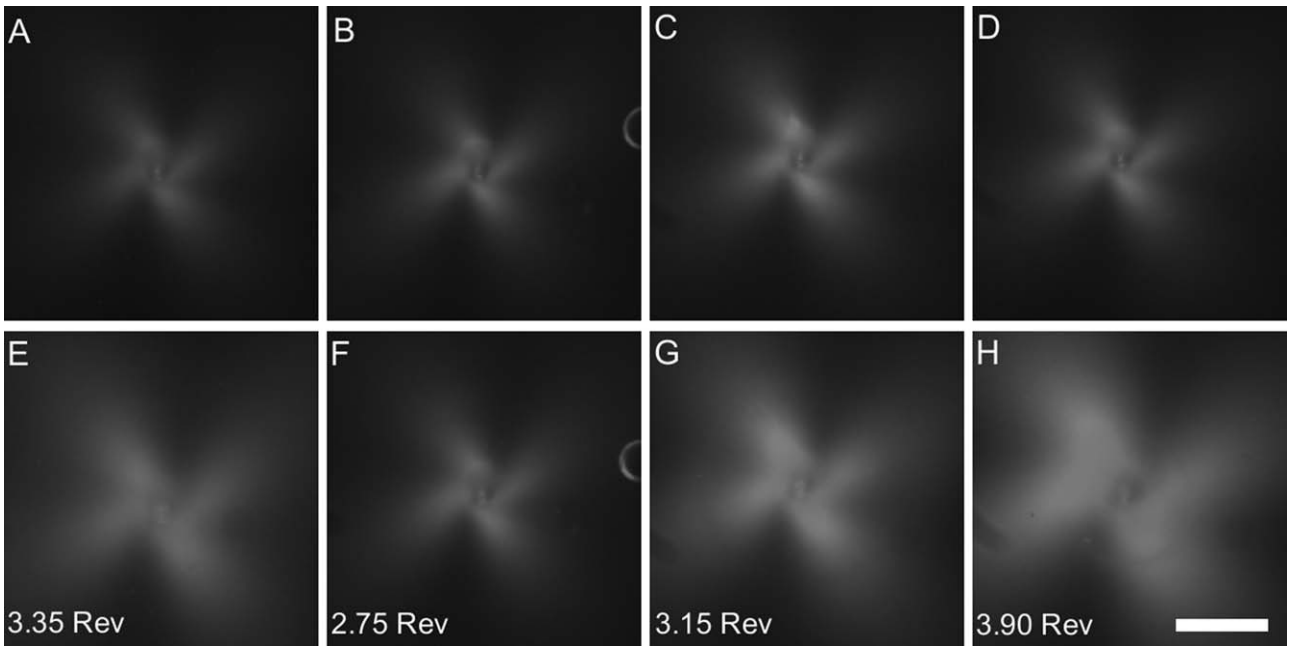

Fig. 6. Representative images of PLM-generated "four-leaf clover" pattern of alignment following *in vitro* acupuncture. (**A**–**D**) Alignment at 2.4 revolutions; (**E**–**H**) Alignment at failure, with number of revolutions at failure indicated in lower-left hand corner. At 2.4 revolutions, alignment-induced birefringence is clearly weaker in the large circular gels (A) and small circular gels (B) when compared with elliptical gels (C) and planar gels (D). At failure, alignment was stronger in large circular gels (E) than small circular ones (F) and approached that in elliptical gels (G), because the large circles were able to withstand more needle rotation before failing. Planar gels (H) demonstrated the strongest field of alignment at failure. Bar: 1 mm.

Failure of the gels consistently presented as a tearing within the body of the gel, and did not occur at the interface with the needle or at the interface with the PPE wall. Statistical comparison with ANOVA indicated that assay geometry significantly affected the number of revolutions before failure ($P < 0.001$) and the alignment at failure ($P < 0.001$). Posthoc pairwise comparisons of revolutions-to-failure with the Hochberg GT-2 method revealed that the smaller circular gels failed at the lowest number of revolutions, followed by the elliptical gels, the large circular gels, and finally the planar gels (all pairwise comparisons significant with max $P = 0.023$) (Fig. 7B). Posthoc pairwise comparisons of alignment at failure with the Hochberg GT2 test demonstrated that the planar gels had the greatest alignment at failure ($P < 0.001$ for pairwise comparisons against each of the other groups); alignment at failure between the elliptical and large circular assays was statistically indistinguishable ($P = 0.910$), and alignment was least in the small circular gels ($P < 0.001$ for all pairwise comparisons against other configurations; Fig. 7C).

Effects of Assay Geometry on Alignment Pattern

The initial coincident orientation of the crossed polars with respect to the assay axes generated a PLM image of fiber alignment with a prevailing orientation of 45° to the major and minor axes of the elliptical gel (or the vertical and horizontal axes of the circular gels; Figs. 5, 8). For these cases, each of the four "clover leafs" was roughly equal in shape and size because of the symmetry of the four quadrants of alignment with respect to the geometry. By rotating the crossed polars, alignment in other directions was assessed. The degree of anisotropy of the clover pattern was described as the ratio of the size of the leafs on perpendicular axes (Fig. 8G). As the orientation was changed, the circular gels still presented largely uniform alignments, and no statistical differences were identified in the asymmetry ratio among the different axes of orientation (ANOVA, $P = 0.087$ for the larger circular gels; $P = 0.424$ for the small circular gels). However, the alignment image in the planar and elliptical gels was nonuniform, with significantly stronger alignment occurring in the direction of the minor axis when compared with the circular gels, which was consistent with a stronger alignment field in a smaller circular assay (ANOVA, $P < 0.001$ for elliptical and planar gels). Posthoc pairwise comparisons of the ratio of asymmetry with Hochberg GT2 test indicated significant increases as the polarization axes were rotated 22.5° and 45° ($P < 0.001$ for all pairwise comparisons) for both the elliptical and planar gels.

Effects of Assay Geometry on Cell Alignment

Fibril and cell alignment in cell-populated gels was consistent with the fiber alignment observed in acellular gels. Fibril and cell alignment appeared stronger along the minor axis of the elliptical gels but was uniform in circular gels, and, in both cases, extended several millimeters away from the needle (Fig. 9), and, in some cases, to the boundary of the assay (up to 14 mm away from the needle) even though needling was limited to only two revolutions. To quantify cell alignment, an alignment index, Φ was calculated for each cell in a z-stack of images that encompassed a volume of $\sim$2.0 mm^3 around the needle position and plotted at the cell centroid (Fig. 10). Before needling, cells were randomly aligned, and the average value of Φ was close to the

ideal value for random alignment of 0.5. After needling of circular gels, cells were primarily oriented radially, and the alignment was uniform with respect to angular position at the same radius. In elliptical gels, radial alignment occurred preferentially along the minor axis, and cells within the remainder of the gel appeared to be aligned randomly. Statistical comparison of average alignment values demonstrated that cells in both circular and elliptical gels became significantly more aligned after needling ($P < 0.001$). Cell number in the imaged region also increased significantly in the needled gels ($P < 0.001$), which coincided with the substantial displacement of fibers toward the needle. Within circular gels, cell density in the imaged region appeared to be uniform with respect to circumferential position but was greater along the minor axis within elliptical gels.

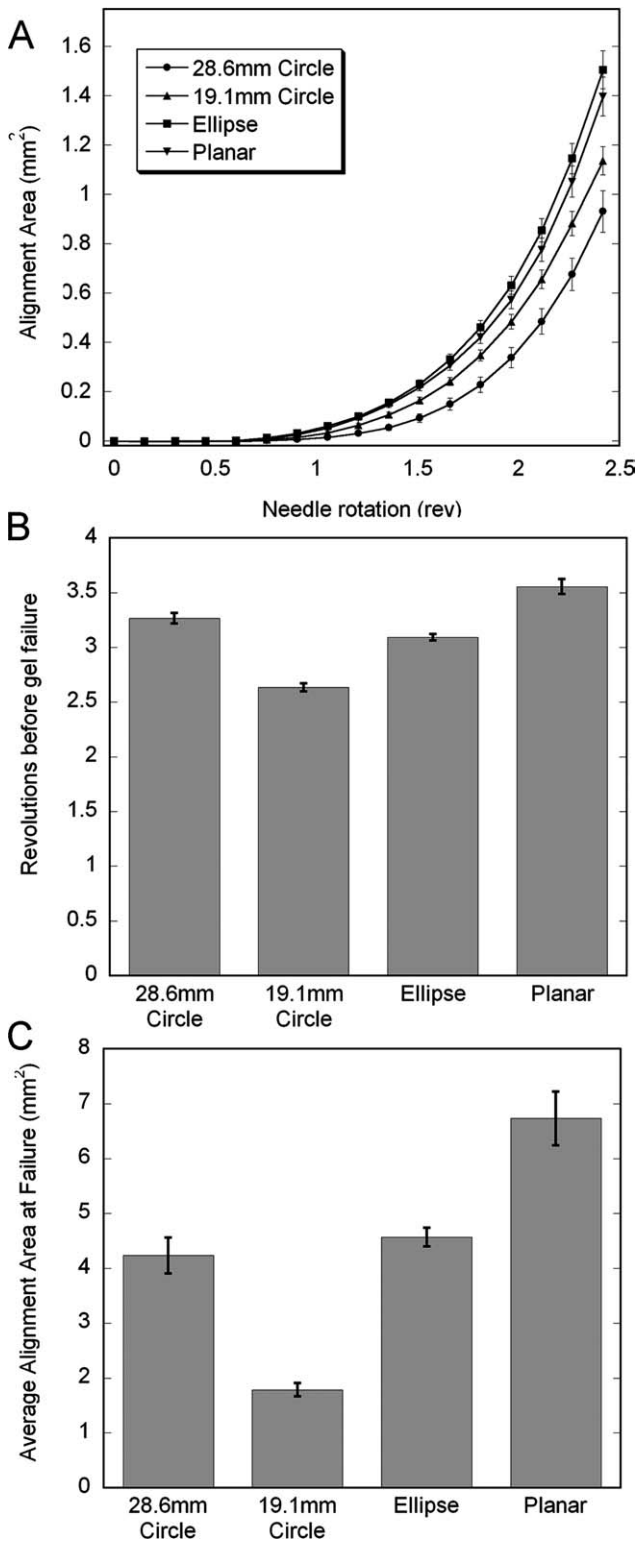

Fig. 7. Effects of assay geometry on gel failure and fiber alignment. (**A**) Evolution of alignment area (average ± standard error) up to 2.4 revolutions, which represented the fewest revolutions before failure across all conditions. (**B**) Average revolutions (±standard error) before gel failure. (**C**) Average alignment area (±standard error) at failure. Small diameter circular gels generated more alignment per revolution that larger gels but also failed earlier, and the alignment at failure was greater for the larger gels. Introducing a nonuniform boundary condition significantly affected both alignment and failure. Fibers in the elliptical geometry aligned faster than in either circular assay but failed in between the two. The net alignment at failure was the same statistically as that produced in the large circles. When the anisotropy was increased with the planar gels, gels aligned at the same rate as in the ellipses but were able to withstand the most number of revolutions before failure (Hochberg GT2 test, $P < 0.001$), which enabled the planar gels to demonstrate the greatest alignment at failure ($P < 0.001$).

DISCUSSION

Recent research has suggested a role for loose connective tissue located along intermuscular and intramuscular fascial planes in transferring mechanical signals imparted by needle manipulation to resident cells via displacement and deformation of the tissue. In humans, in addition to increased amounts of loose connective tissue, these planes also present a distinct geometry compared with "control" locations (Langevin and Yandow, 2002). For the same number of needle rotations, the "grasping" force is greater when therapy is applied at acupuncture points located above a fascial plane than at control points located above skeletal muscle (Langevin et al., 2001b). Using simple *in vitro* analogs, we demonstrated that the geometric constraints present in the narrowing channels of connective tissue at fascial cleavage planes may act to accentuate the mechanical response of the tissue to needle manipulation.

When considering the anatomical organization of loose connective tissue (e.g., Fig. 1), the tissue at control points above skeletal muscle is effectively unbounded, whereas the connective tissue at acupuncture points is bounded by muscle groups. Although not to the same disparity, we believe that we captured the essence of this distinction in boundary conditions by altering the shape and size of the collagen gel. We used two metrics as indices of the mechanical response—collagen fiber alignment and gel failure. The strength of alignment—demonstrated as brighter regions in PLM—is a function of the orientation of fibers and the number/density of oriented fibers. We found that alignment was stronger when boundaries were closer to the needle, which is not surprising. It is well documented that anisotropic deformations of fibrillar materials, such as collagen gels, generates fiber alignment that is dependent on the magnitude of the disparity of deformation in different directions (Barocas and Tranquillo, 1997a, b). Needle rotation in circular gels causes uniform winding of collagen fibers around

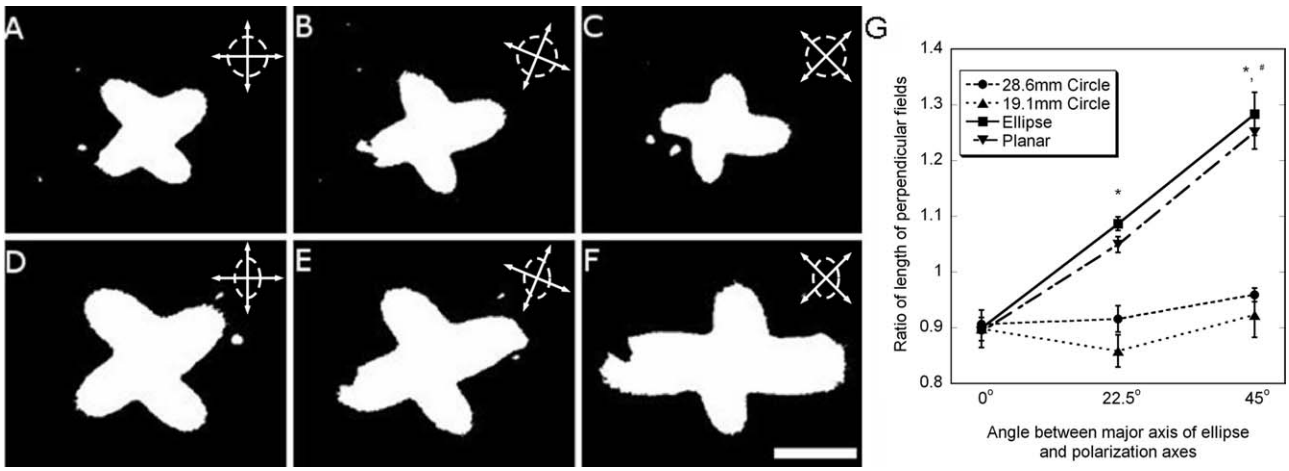

Fig. 8. Effects of changing the orientation of the polarization axes (cross in upper right-hand corner) with respect to the assay geometry (large circle **A**–**C**; or ellipse **D**–**F**, shown) on the clover-leaf pattern after binarizing the images with the threshold algorithm. Within circular gels with uniform boundaries, the clover-leaf patterns remained symmetric regardless of the polarization axes. Patterns within elliptical and planar gels were symmetric when the axes were coincident with the major and minor axes but became increasingly asymmetric as the angle was changed to 22.5° (E) and 45° (F). The degree of asymmetry was expressed as the ratio of the length of perpendicular (opposite) leafs in each assay geometry (**G**). The elliptical and planar geometries became increasingly asymmetric as the polarization axis was rotated (*, significantly different than 0°; #, significantly different than 22.5°, ANOVA followed by pairwise comparisons with Hochberg's GT-2 method.) Bar: 1 mm.

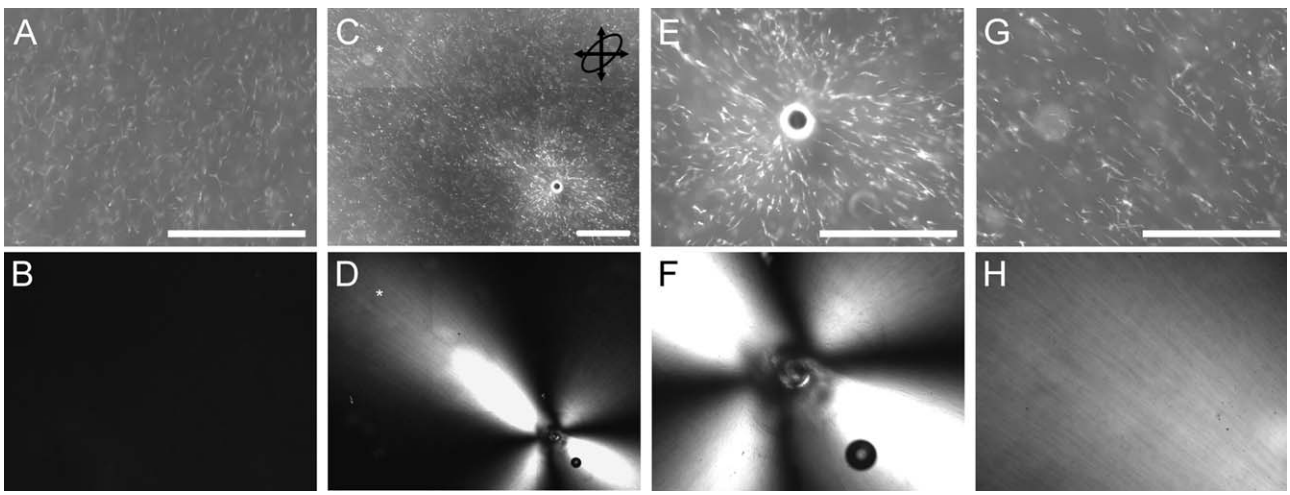

Fig. 9. Epifluorescence images of GFP-expressing fibroblasts (top) and polarized light images of fiber orientation (bottom) in elliptical gels demonstrate that cell alignment follows fiber alignment. Before needle rotation, cells appeared randomly oriented (**A**), and PLM images are uniformly dark (**B**). After two needle rotations, significant alignment of cells (**C**) and fibers (**D**) is observed, particularly in the direction of the minor axis of the ellipse (shown in upper right-hand corner of C). A higher magnification image of cell alignment near the needle (**E**) demonstrates radial alignment that falls off faster in the major axis direction than the minor axis direction, which correlates to the corresponding PLM image of fiber alignment (**F**). The alignment is propagated along the minor axis several millimeters away from the needle (*, in C and D, shown at high magnification in **G** and **H**). Bar: 1 mm.

the needle, drawing in fibers from the surrounding gel. At the perimeter, these fibers are constrained via intercalation with the PPE wall, thereby preventing circumferential movement. As a result, the fibers throughout the bulk of the gel straighten radially, and the closer the boundary is to the needle, the faster these fibers align. As the distance to the boundary constraint is uniform around the perimeter, the alignment field is isotropic with respect to radial position. Coincident with development of the uniform alignment is an increase in stress in the system that is also uniform. Accordingly, the circular gels with smaller diameter fail after fewer needle revolutions than the larger circular gels.

When the boundary is nonuniform, as with the elliptical or planar gels, there is greater resistance to displacement along the minor axis or across the plane. The fibers not only align radially, but also accumulate along the minor axis to become denser and generate a stronger alignment signal, thereby, resulting in nonuniform alignment measurements with respect to angular position, as was demonstrated by rotating the polarization axes. The stronger alignment in the "shorter" direction was consistent with results from the circular gels and the anisotropy predicted by simple mechanics. The allowance for displacement appeared to shield the gel from failure

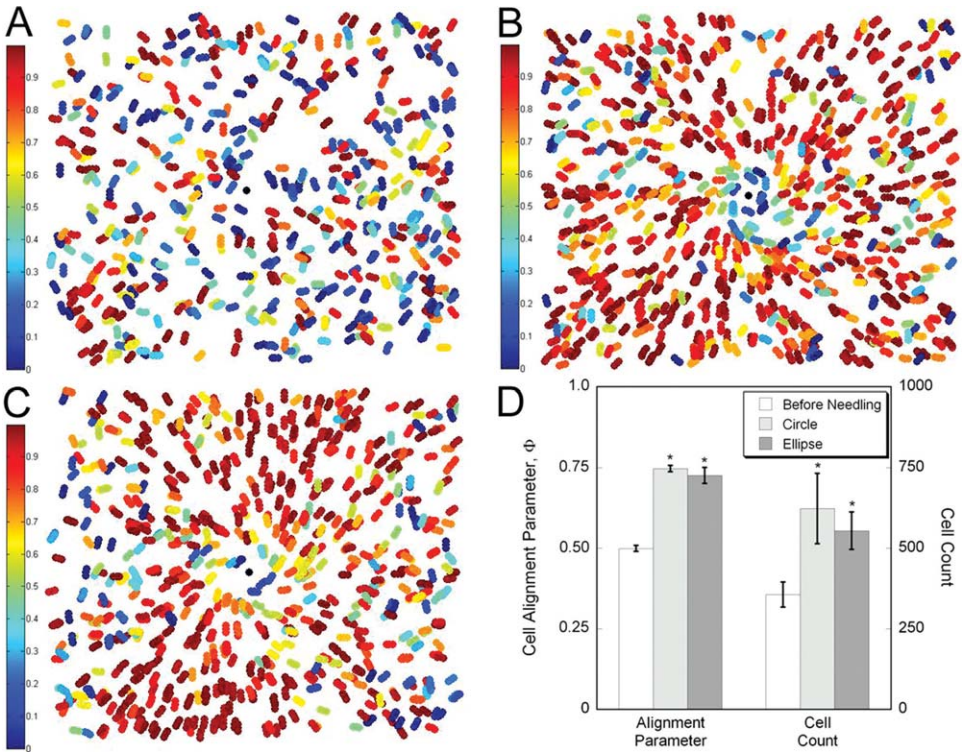

Fig. 10. Quantitative assessment of the cell alignment parameter, Φ, which ranges from 0 (circumferential alignment—blue) to 1 (radial alignment—red). The alignment parameter was calculated for each cell in a stack of images encompassing a volume of ~2.0 mm^3 taken with a 4× objective and projected onto the same plot (~2.25 × 1.25 mm^2). Representative plots are shown for gels before needling (**A**), and after needling in circular (**B**) and elliptical (**C**) gels, where the major axis is oriented horizontally. The black circle in the middle represents the needle location. Before needling, cells are randomly oriented. After needling, alignment increases in both circular and elliptical gels. Some circumferential alignment is apparent near the needle, but the prevailing orientation is radial. The radial alignment is uniform throughout the imaged field in circular gels. In elliptical gels, radial alignment is preferentially seen in the direction of the minor axis. (**D**) The average alignment in the different conditions was significantly greater after needling than before needling, where Φ was approximately the predicted value of 0.5 for random alignment. The average cell count in the imaged area also increased after acupuncture needle rotation, demonstrating the significant displacement of cells and collagen toward needle as the fibers wind around the needle. (*, significantly different than before needling, ANOVA followed by pairwise comparisons with Hochberg GT2 method.)

as well. Elliptical gels failed after a greater number of needle revolutions than the small circular gels, despite demonstrating greater alignment. Planar gels demonstrated an even greater resistance to failure, surpassing even the larger circle. As in our previous study (Julias et al., 2008), in all gels, the failure occurred within the belly of the gel, approximately where circumferential alignment transitions to radial alignment, which places the fibers under a significant shear load.

When fibroblasts were included in the gels, the cells aligned to follow the collagen fibers, similarly to that observed in rat and mouse full-thickness tissue explants (Langevin et al., 2001a). This phenomenon is known as contact guidance, which is generally defined as the tendency for cells to align and/or migrate preferentially in the direction of the prevailing orientation of the underlying substrate or surrounding network. As such, fiber alignment produced by an anisotropic mechanical strain field will also induce alignment of cells via contact guidance (Girton et al., 2002). Cell alignment in the circular gels was circumferential near the needle, and then became radial, and was uniform with respect to angular position. The elliptical gels also produced circumferentially aligned cells near the needle, but radial alignment was more prevalent along the minor axis of the ellipse. Coincident with the significant increase in alignment was an increase in cell density in the volume of tissue near the needle, which resulted from the convective transport of cells along with the displaced tissue toward the needle.

Despite large areas along the major axis that lacked alignment in this region, the average cell alignment and cell number in the elliptical gels were the same as the circular gels, which also points to the relatively greater displacement of the tissue toward the minor axis in the elliptical assay than in the circular ones. Cell alignment consistently extended several millimeters away from the needle, and, in some cases, to the boundary of the assay. This is particularly noteworthy, as the cellular gels were only subjected to two needle revolutions, where fiber alignment began to sharply increase with further needle rotation (Fig. 7).

Together with our previous *in vitro* study, these results provide quantitative illustrations of some of the distinct features of loose connective that help to explain its unique capabilities to transfer mechanical load during acupuncture therapy. Specifically, the anisotropic boundaries presented within connective tissue planes appear to allow a greater volume of fibrous tissue to be displaced and deformed and shields that tissue from tearing, thereby, increasing the mechanical stimulus introduced during therapy. These locations

also have more of the loose connective tissue, which can further accentuate the response. Another factor that may affect the biophysical response that may be added to the *in vitro* model is the extracellular matrix composition. Loose connective tissue maintains a significant proteoglycan content (Bode-Lesniewska et al., 1996; Stoeckelhuber et al., 2002), which can affect bulk and micromechanical properties and potentially cell-matrix adhesion. Thus, tissue composition may further distinguish connective tissue from surrounding tissues *in vivo*, and also may change with aging and disease to alter the tissue response of a particular patient (or a location on that patient) to needle manipulation.

Studies by Langevin (Langevin et al., 2005; Langevin et al., 2006; Langevin et al., 2007) have demonstrated that this mechanical stimulus can induce morphologic and phenotypic changes in fibroblasts, and there is a growing body of literature that substantiates the role of mechanotransduction in dictating cellular physiology and pathophysiology (Eshel and Lanir, 2001; Grinnell, 2003; Grinnell et al., 2003; Stegemann and Nerem, 2003; Bride et al., 2004). However, if these signals generated during acupuncture needling can be propagated along meridians, and whether the mechanical signals play a role in the therapeutic benefits, remain to be elucidated. In this study, even after only two needle revolutions, cells (and fibers) were aligned several millimeters away from the needle, and manipulations *in vivo* are typically more substantial (Langevin et al., 2004; Langevin et al., 2006). The results demonstrating stronger fiber alignment (and presumably mechanical signaling) in the narrower direction in our assays suggests that the signal generated by a single needle would be better propagated across a connective tissue plane rather than along the plane. However, the increase in cell and fiber density results from recruitment and displacement along the tissue plane. Moreover, these results point to the crucial role of boundary conditions in enabling fiber winding. Not every position along a connective tissue plane is recognized as an "acupuncture point," and a more precise examination of the mechanical barriers at these locations is warranted. Furthermore, in a clinical setting, acupuncture therapy most often involves manipulation of multiple needles along a plane (Yamashita et al., 2001; Eshkevari, 2003), which could further introduce constraining boundaries to tissue displacement and alter the strength and direction of mechanical stimulation.

ACKNOWLEDGMENTS

Data from the Visible Human Project Initiative was made available through the National Library of Medicine and the University of Colorado.

LITERATURE CITED

Barocas VH, Tranquillo RT. 1997a. An anisotropic biphasic theory of tissue-equivalent mechanics: the interplay among cell traction, fibrillar network deformation, fibril alignment, and cell contact guidance. J Biomech Eng 119:137–145.

Barocas VH, Tranquillo RT. 1997b. A finite element solution for the anisotropic biphasic theory of tissue-equivalent mechanics: the effect of contact guidance on isometric cell traction measurement. J Biomech Eng 119:261–268.

Bode-Lesniewska B, Dours-Zimmermann MT, Odermatt BF, Briner J, Heitz PU, Zimmermann DR. 1996. Distribution of the large aggregating proteoglycan versican in adult human tissues. J Histochem Cytochem 44:303–312.

Bride J, Viennet C, Lucarz-Bietry A, Humbert P. 2004. Indication of fibroblast apoptosis during the maturation of disc-shaped mechanically stressed collagen lattices. Arch Dermatol Res 295:312–317.

Eisenberg D, Davis R, Ettner S, Appel S, Wilkey S, Rompay M, Kessler R. 1998. Trends in alternative medicine use in the United States, 1990–1997. JAMA 280:1569–1575.

Eshel H, Lanir Y. 2001. Effects of strain level and proteoglycan depletion on preconditioning and viscoelastic responses of rat dorsal skin. Ann Biomed Eng 29:164–172.

Eshkevari L. 2003. Acupuncture and pain: a review of the literature. Aana J 71:361–370.

Girton T, Barocas V, Tranquillo R. 2002. Confined compression of a tissue-equivalent: collagen fibril and cell alignment in response to anisotropic strain. Journal of Biomechanical Engineering 124:568–575.

Grinnell F. 2003. Fibroblast biology in three-dimensional collagen matrices. Trends Cell Biol 13:264–269.

Grinnell F, Ho C, Tamariz E, Lee D, Skuta G. 2003. Dendritic fibroblasts in three-dimensional collagen matrices. Mol Biol Cell 14:384–395.

Helms JM. 1995. Acupuncture energetics—a clinical approach for physicians. Berkeley, CA: Medical Acupuncture.

Julias M, Edgar LT, Buettner HM, Shreiber DI. 2008. An in vitro assay of collagen fiber alignment by acupuncture needle rotation. Biomed Eng Online 7:19.

Knapp DM, Helou EF, Tranquillo RT. 1999. A fibrin or collagen gel assay for tissue cell chemotaxis: assessment of fibroblast chemotaxis to GRGDSP. Exp Cell Res 247:543–553.

Langevin HM, Bouffard NA, Badger GJ, Churchill DL, Howe AK. 2006. Subcutaneous tissue fibroblast cytoskeletal remodeling induced by acupuncture: evidence for a mechanotransduction-based mechanism. J Cell Physiol 207:767–774.

Langevin HM, Bouffard NA, Badger GJ, Iatridis JC, Howe AK. 2005. Dynamic fibroblast cytoskeletal response to subcutaneous tissue stretch ex vivo and in vivo. Am J Physiol Cell Physiol 288:C747–C756.

Langevin HM, Bouffard NA, Churchill DL, Badger GJ. 2007. Connective tissue fibroblast response to acupuncture: dose-dependent effect of bidirectional needle rotation. J Altern Complement Med 13:355–360.

Langevin HM, Churchill DL, Cipolla MJ. 2001a. Mechanical signaling through connective tissue: a mechanism for the therapeutic effect of acupuncture. Faseb J 15:2275–2282.

Langevin HM, Churchill DL, Fox JR, Badger GJ, Garra BS, Krag MH. 2001b. Biomechanical response to acupuncture needling in humans. J Appl Physiol 91:2471–2478.

Langevin HM, Churchill DL, Wu J, Badger GJ, Yandow JA, Fox JR, Krag MH. 2002. Evidence of connective tissue involvement in acupuncture. Faseb J 16:872–874.

Langevin HM, Konofagou EE, Badger GJ, Churchill DL, Fox JR, Ophir J, Garra BS. 2004. Tissue displacements during acupuncture using ultrasound elastography techniques. Ultrasound Med Biol 30:1173–1183.

Langevin HM, Yandow JA. 2002. Relationship of acupuncture points and meridians to connective tissue planes. Anat Rec 269:257–265.

NIH Consensus Statement. 1997. Acupuncture. Bethesda, MD: NIH. Vol. 15: p1–34.

Shreiber D, Enever P, Tranquillo R. 2001. Effects of PDGF-BB on rat dermal fibroblast behavior in mechanically stressed and unstressed collagen and fibrin gels. Exp Cell Res 266:155–166.

Sokal RR, Rohlf FJ. 1981. Biometry. New York: W.H. Freeman and Company.

Stegemann J, Nerem R. 2003. Phenotype modulation in vascular tissue engineering using biochemical and mechanical stimulation. Ann Biomed Eng 31:391–402.

Stoeckelhuber M, Stumpf P, Hoefter EA, Welsch U. 2002. Proteoglycan-collagen associations in the non-lactating human breast connective tissue during the menstrual cycle. Histochem Cell Biol 118:221–230.

Yamashita H, Tsukayama H, White AR, Tanno Y, Sugishita C, Ernst E. 2001. Systematic review of adverse events following acupuncture: the Japanese literature. Complement Ther Med 9:98–104.